

Unlocking the Potential of Synthetic Fuel Production: Coupled Optimization of Heat Exchanger Network and Operating Parameters of a 1 MW Power-to-Liquid Plant

David Huber^{a,*}, Felix Birkelbach^a, René Hofmann^a

^a*TU Wien, Institute of Energy Systems and Thermodynamics, Getreidemarkt 9/BA, 1060 Vienna, Austria*

Abstract

The use of synthetic fuels is a promising way to reduce emissions significantly. To accelerate cost-effective large-scale synthetic fuel deployment, we optimize a novel 1 MW PtL-plant in terms of PtL-efficiency and fuel production costs. For numerous plants, the available waste heat and temperature level depend on the operating point. To optimize efficiency and costs, the choice of the operating point is included in the heat exchanger network synthesis. All nonlinearities are approximated using piecewise linear models and transferred to MILP. Adapting the epsilon constraint method allows us to solve the multi-criteria problem with uniformly distributed solutions on the Pareto front. We improved the lowest production costs of 1.89 €/kg and the highest efficiency of 58.08 % from the conventional design process to 1.83 €/kg and 61.33 %. By applying the presented method, climate-neutral synthetic fuels can be promoted and emissions can be reduced in the long term.

Keywords: synthetic fuels, power-to-liquid, mixed integer linear programming, heat exchanger network synthesis, multi-criteria optimization

1. Introduction

The transport sector contributed 7.98 Gt of CO₂, equivalent to about 23 % of global CO₂ emissions, in 2022 [1]. Reducing these emissions is crucial for achieving climate goals. Electrification of the transport sector will enable a significant reduction in climate-damaging emissions. Projections by the IEA indicate that the share of electric vehicles will increase from 1.5 % in 2021 to about 30 % by 2030 and more than 60 % by 2050 [2]. Electrification is not possible for the entire transport sector. There is still no viable alternative to liquid fuels for maritime

*Corresponding author

Email address: david.huber@tuwien.ac.at (David Huber)

and aviation. Heavy machines such as snow groomers or agricultural machinery are similarly affected by a lack of climate-neutral powertrain systems. Synthetic fuels, or e-fuels, can be used directly in existing combustion engines as a drop-in solution to achieve climate neutrality. Compared to other climate-neutral fuels like hydrogen, using e-fuels offers the advantages of cheap transport and storage costs and existing infrastructure can be continued to be used.

1.1. Synthetic Fuel Production

The production of synthetic fuels involves multiple chemical conversion steps of mainly CO_2 , H_2O and renewable electricity sources like wind, solar or photovoltaic. The CO_2 can be provided through different routes like capturing CO_2 from the atmosphere with direct air capture (DAC), water, biomass, or flue gas [3]. Simplified, electrolysis reduces H_2O to a hydrogen-rich synthesis gas. In a subsequent step, the gas is synthesized with purified CO_2 in a Fischer-Tropsch (FT) reactor. The hydrocarbons from the FT-reactor are then separated into different fractions such as naphtha, diesel and waxes.

Even though the key components such as electrolysis and FT-reactor are already commercially available, only a few plants are still in operation [4, 5]. The first commercial PtL-plant build was the Haru Oni in Punta Arenas, Chile [6]. Methanol is produced using DAC and a polymer electrolyte membrane (PEM) electrolysis system powered by renewable electricity from a 3.4 MW wind turbine. During the pilot phase in December 2022, the first barrel of synthetic fuel could already be filled. The production is to be increased to 130 000 L in March 2023. The Norsk e-fuel plant in Mosjøen Norway is expected to produce up to 50 million liters of kerosene for aviation with renewable electricity from wind and hydropower as early in 2026 [7]. The CO_2 required for the solid oxide electrolysis cell (SOEC) is supplied by DAC. According to Norsk e-fuel, three production facilities are expected to produce more than 250 million liters annually by the end of 2030. The George Olah plant in Svartsengi, Iceland, can produce up to 4000 tons (about 5 million liters) of methanol annually [8]. A nearby geothermal power plant's off-gas provides the CO_2 feedstock. The alkaline water electrolysis is fed entirely renewably from the Icelandic power grid. INERATEC's PtL-plant in Karlsruhe, Germany, is expected to produce about 3500 tons (about 4.6 million liters) of synthetic kerosene and diesel per year, starting in 2023 [9]. Feedstocks are up to 10 000 tons of biogenic CO_2 per year and renewable electricity.

The production of e-fuels is still in its earliest stage and significant challenges still need to be overcome [10]. The central problem is that production costs are currently too high, which means that the fuel cannot be used in an economically viable way for end users [11]. Ueckerdt et al. [12] have estimated production costs of 3.2 €/L for gasoline from 2020 to 2050. Ram et al. [13] have estimated production costs of 1.14 €/L for the year 2050. This forecast refers to all FT-products. However, depending on the FT-reactor, the share of gasoline is only about a third, which again leads to an estimate similar to that of Ueckerdt et al. Based on the investment costs of the demonstration plant in Haru Oni, Chile, a current production price of about 50 €/L results. In contrast, the average

wholesale price of fossil gasoline in 2021 was about 0.5 €/L [14]. A CO₂ price of about 1000 €/tCO₂ would have to be introduced to create cost equality [15]. According to Ueckerdt et al. [15], production costs of about 1 €/L will occur in the long term, which will make the fuel interesting for end users. Large and, above all, plants with low production costs and high efficiency must be built to achieve this price target.

1.2. Plant Design & Operation

Complex plants like a PtL-plant are composed of several units. At the design stage of a plant, the size of the units is primarily determined by the intended capacity of the plant. Standard manufacturers' sizes are used to reduce costs by buying off-the-shelf units. To guarantee the proper operation of the plant and the units, process engineers use commercial software such as Aspen HYSYS or IPSEpro. Due to the large number of units interacting with each other, many independent operating parameters result, which makes it challenging to find an optimal operating point empirically. Therefore, the plant's performance is highly dependent on the knowledge and experience of the process engineers. From an engineering point of view, it is necessary to use optimization methods to utilize the system's full potential. In contrast to commercial software, operational optimization enables the minimization of certain criteria like costs or emissions to find an optimal operation point. Al-Rashed & Afrand [16], for example, used a genetic algorithm (GA) to optimize the exergetic and economic efficiency of a combined gas turbine and supercritical CO₂ cycle for power production. They were able to find an optimal operating point with 25.3 % higher exergetic efficiency and achieved 24.6 % cost savings resulting from optimized inlet cooling of the compressor. Cao et al. [17] compared biomass gasification and digestion for a combined biomass to power and hydrogen plant. The units' characteristics were modeled to represent emissions, efficiency and levelized cost of product (LCOP) criteria and optimized with a GA. The results do not indicate a preferred system design. However, modeling the components depending on the operating point could create a holistic basis for decision-making. Hai et al. [18] optimized the operation of a solar-geothermal energy system providing electricity and hydrogen using GA. Optimizing the operating point of the components increased the power output by 500 kW to 4.099 MW. At the same time, the production of H₂ was increased from 8 g/s to 29 g/s. Wang et al. [19] optimized the operation strategy of a solar tower power plant using particle swarm optimization. They increased the daily power generation by 13.4 %.

The literature cited earlier shows the great potential of optimizing operating characteristics. However, these methods are limited because the heat exchanger network (HEN) design is neglected. The HEN design is a crucial factor for cost and energy savings, especially in plants where much energy is necessary for heating and cooling process streams. Commercial software can be used to simulate an existing HEN. However, the optimal interconnection must be specified by the process engineers. The empirical rules of pinch analysis are often used [20]. A promising approach for finding an optimal HEN is the heat exchanger network synthesis (HENS). With HENS, an optimal heat exchanger configuration can be

found using mathematical programming subjected to given stream parameters such as temperatures and heat capacity flows. Some representative use cases and the achievable potential for cost and energy savings can be found in the publications of, for example, Yee & Grossmann [21], Escobar et al. [22] and Liu et al. [23].

A significant limitation of HENS is that a defined operating point and, as a result, constant stream parameters are assumed. In cases where the operating point affects the temperatures and flow capacities of the streams, the operating behavior cannot be covered by classical HENS. In contrast, when the operating point is optimized, a predefined configuration of the HEN is necessary. Since the operating point influences the HEN and vice versa, optimizing HEN and the operating point simultaneously will lead to better results. In contrast to flexible HEN design methods, in this paper, we do not optimize the HEN for different operating points. With our method, the operating point and the HEN are optimized simultaneously.

1.3. Novelty & Contribution

In this work, we close a research gap by coupling the optimization of the HEN and operating parameters. Our method allows us to overcome design and operational optimization weaknesses and enforce both approaches' strengths. To exploit the potential of modern MILP solvers, we use piecewise linear approximations and efficient logarithmic coding. Applying an adapted epsilon constraint method enables the consideration of the trade-off between high process efficiency and low production costs. Therefore, decision-makers and process engineers can be provided with a holistic foundation for the process design.

Our method is demonstrated on a novel 1 MW PtL-plant. As a step towards large-scale industrial production, the goal is to design a medium-sized PtL-plant successfully. For a given electrolyzer size of 1 MW, the aim is to produce as much synthetic fuel as possible cost-effectively and efficiently simultaneously. Therefore, we present how to formulate the efficiency and production cost objective functions. To evaluate our method's potential, the results from coupled optimization are compared to results from the traditional plant design approach, where only the HEN is optimized. The results show that synthetic fuels can be produced with minimal production costs of 1.83 €/kg or at the highest efficiency of 61.84 %. The decarbonization of the transport sector can thus be accelerated and emissions can be avoided.

1.4. Paper Organization

The novel 1 MW PtL-plant studied is described in Section 2.1. In Section 2.2, we show the basic concept of the adapted HENS superstructure, the piecewise linear approximation, the logarithmic coding approach for an efficient transfer to MILP, and our adaptations to the epsilon constraint method. Since implementing the operating point dependent stream parameters is specifically tailored to the use case, the modeling is discussed in detail in Section 3. In Section 4, we show the results of our method in comparison to an optimization of the HEN only.

2. Materials & Methods

2.1. System Description

As part of the *IFE* (de.: Innovation Flüssige Energie, eng.: Innovation Liquid Energy) research project, a novel PtL-plant is designed. The PtL-plant will be designed to a maximum electrolysis capacity of approximately 1 MW and will produce climate-neutral fuels for the transport sector. Water, renewable electricity, exhaust gas from a cement plant and air are used as feedstock. In Figure 1, the PtL-plant is schematically shown with its five main components: steam generation, CO₂ conditioning, high-temperature solid oxide co-electrolysis (co-SOEC), Fischer-Tropsch (FT) reactor with upgrading and combustion system. For simplicity, no valves, pumps, or compressors are shown. Heat exchangers indicate the heat transfer points of the HEN. The cold process streams, which must be heated, are shown in blue. Hot process streams must be cooled down and shown in red. In the following sections, the central components are briefly discussed.

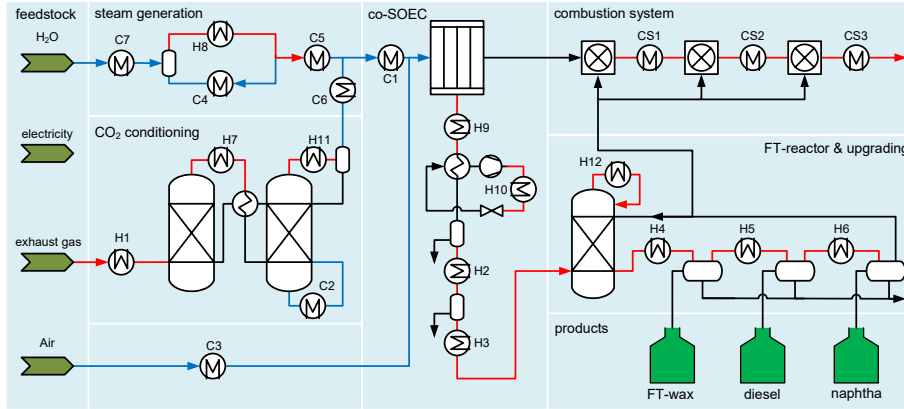


Figure 1: Schematic representation of the 1 MW PtL-plant with the five main components: steam generation, CO₂ conditioning, co-SOEC, FT-reactor with upgrading and combustion system.

2.1.1. Steam Generation

The steam generator is fed with pure water at 20 °C. The conditioned water is preheated, evaporated and superheated by the heat exchangers in streams C7, C4 and C5.

2.1.2. CO₂ Conditioning

Due to the high energy consumption for the supply of CO₂ in sufficient purity, the quality of the CO₂ source is an essential parameter for the design. In this case, exhaust gas from a cement plant is used due to the high CO₂ concentration. The exhaust gas enters the conditioning with 15.17 wt% CO₂, 81.11 wt% N₂ and 3.72 wt% H₂O and a temperature of 40 °C. To control the

temperature for adsorption and desorption, the hot streams H7 and H11 must be cooled and the cold stream C2 heated. At the end of the conditioning process, the CO₂ has a purity of 98.73 wt% and a low residual content of water.

2.1.3. Co-SOEC

The central element of the PtL-process is the co-SOEC. The conditioned CO₂ is superheated within stream C6 and mixed with the superheated steam. Within stream C1, the mixture is further superheated to the operating temperature of the co-SOEC. Both are reformed with preheated air at temperatures between 800 and 900 °C to an H₂-rich gas and CO. Before entering the FT reactor, the synthesis gas leaving the co-SOEC is cooled in four stages and condensed constituents are separated. A compressor-based cooling system supports the second cooling stage.

With a maximum power of approx. 1 MW, the co-SOEC is the largest electricity consumer in the system. The cell voltage has a strong influence on the overall power consumption and subsequently on the efficiency and production costs.

2.1.4. FT-Reactor & Upgrading

In the FT-reactor, the synthetic gas from the co-SOEC is passed over a catalyst at high temperature and pressure. In the subsequent upgrading process, the FT-syn crude is separated into the fractions FT-wax, diesel and naphtha and prepared for final use. The unreacted synthesis gas is partially recirculated and fed to the combustion system. The product properties downstream of the upgrading are given in Table 1.

Table 1: Chemical and physical product properties at 40 °C and 101 324.97 Pa downstream the upgrading.

v	product	$h_{\text{prod}} / \text{MJ/kg}$	$\rho_{\text{prod}} / \text{kg/m}^3$	$\mu_{\text{prod}} / \text{mPa/s}$
1	FT-wax	43.887	797.73	6.7477
2	diesel	44.345	748.81	1.5983
3	naphtha	44.676	516.17	0.5893

2.1.5. Combustion System

The combustion system serves as an internal hot utility and provides energy to heat the cold process streams. The CS consists of three serially connected combustion chambers. The offgas from the separation, which can no longer be recirculated, is used as fuel. Combustion takes place at high air surplus ($\lambda > 150$ for 1st CS; $\lambda > 30$ for 3rd CS). The first combustion chamber is supplied with the entire exhaust air from the co-SOEC. The other two combustion chambers are each fed with the exhaust gas from the combustion chamber in advance.

Since the CS is used as an internal hot utility, the optimal design is a decisive factor for the efficiency of the HEN and the overall process. The selection of the combustion parameters inlet and outlet temperature into the combustion

chamber and fuel mass flow are, in contrast to other processes, not closely linked to technical limitations. Only the material-specific temperature limit of 900°C must not be exceeded. The inlet temperature of the air mainly influences the outlet temperature from the combustion chamber and can be adjusted by the fuel quantity. The inlet temperature results from the streams connected within the HEN. Due to the many freely selectable parameters and the strong influence on the efficiency of the overall process, the design of the CS is a significant challenge for process engineers.

2.2. Methods

In this section, we present the underlying idea behind the coupled optimization of the HEN and operating point. The concept is shown schematically in Figure 2. The physical system composed of two units with two hot and two cold streams is shown at the very top of Figure 2. For simplicity, the heat exchanger network is not illustrated. The operating characteristics of each unit can be reduced to multiple independent operational parameters. It is assumed that a change of the operating parameters leads only to a change of the stream parameters T^{in} , T^{out} and F . Depending on the process, all, none, or only some of the three stream parameters can be affected.

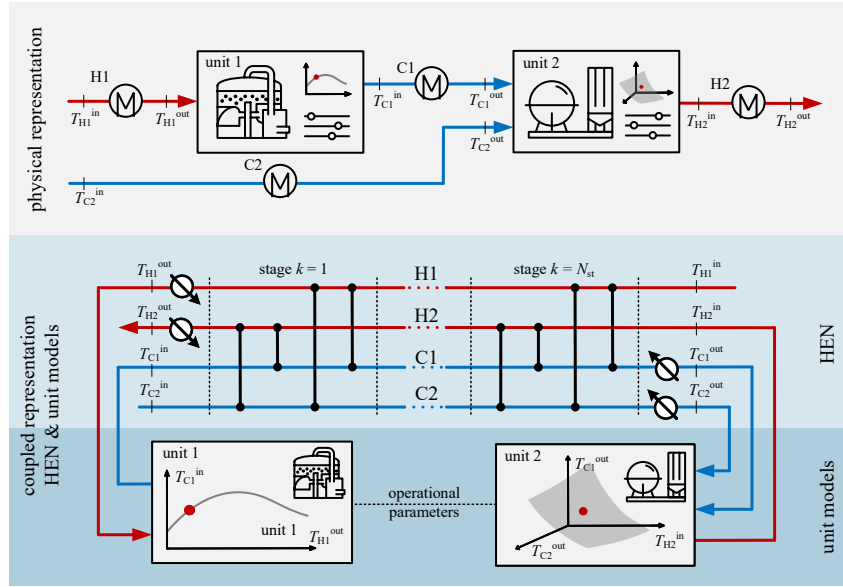


Figure 2: Schematic representation of the method for two units with two hot and two cold streams.

In the middle of Figure 2, the HEN with N_{st} stages and all possible interconnections are shown for the same system. This graph-theoretic representation of

the HEN is based on the superstructure formulation of Yee & Grossman [21]. The heat exchange between the hot and cold streams can occur in N_{st} stages with stream splits. The hot and cold utilities are located at the stream ends.

The coupling between the optimization of the HEN design and the operating point is achieved by implementing models that describe the operating characteristics of the units. In Figure 2, at the bottom, the models of the two units are shown schematically. Each unit has an independent operating variable; in this case, only inlet or outlet temperatures change formulated with variables. The model of unit 1 represents the correlation between the outlet temperature of stream H1 and the inlet temperature of stream C1. The model of unit 2 illustrates the correlation between the outlet temperatures of stream C1 and C2 along with the inlet temperature of stream H2. The objective links the operating variables. The coupled HEN design problem with variable stream parameters is solved using the adapted superstructure formulation of Huber et al. [24].

2.2.1. Linearization

All nonlinearities of the HENS are piecewise linear approximated with superpositioned planes in the two-dimensional. Plane Simplices are used for three-dimensional correlations. Detailed information regarding the methodology can be found in the paper by Huber et al. [24].

Analogously, the units' operating and stream parameters correlations are linearly approximated. The advantage of this method is that the characteristics of the units can be represented with the help of black-, grey- or white-box models. The resulting flexibility in choosing the modeling approach reduces limitations regarding data availability and increases the proposed method's applicability.

2.2.2. Transfer to MILP

All piecewise linear functions are transferred to MILP with the least possible number of binary variables to reduce computation time. One-dimensional, mainly convex curved functions are transferred to MILP without binary variables. All other functions require the use of binary variables. Applying a logarithmic coding approach, according to Vielma and Nemhauser [25], can reduce the number of binary variables to a minimum. Further information about the transfer to MILP can be taken from [24].

2.2.3. Multi-Objective Optimization

The two-objective optimization problem is solved with an adapted epsilon constraint method. As shown in Equation (1), one objective function is minimized and the second is constrained with an upper and lower bound. The epsilon parameters are chosen to be in the range of $f_2^{\min} \leq \varepsilon_i \leq f_2^{\max}$.

$$\begin{aligned} \min \quad & f_1(\mathbf{x}) \\ \text{s.t.} \quad & \varepsilon_i \leq f_2(\mathbf{x}) \leq \varepsilon_{i+1} \quad i = 1, \dots, m \end{aligned} \tag{1}$$

In contrast to the conventional epsilon constraint method, overhanging regions of the Pareto front can be covered. Equidistantly distributed points on the Pareto front can be calculated with minimal computational effort.

3. Modeling

The models are created based on data from steady-state process simulations by project partners using Aspen HYSIS. Modeling is based on the following assumptions:

- The system was simulated with seven different cell voltages between lower ($U_{\text{cell}}^{\text{min}} = 1.275 \text{ V}$) and the upper technical limit ($U_{\text{cell}}^{\text{max}} = 1.305 \text{ V}$).
- The stream parameters T^{in} , T^{out} and F are only dependent on the cell voltage U_{cell} .
- The stream parameters of the CS are independent of the cell voltage. Temperatures and heat capacity flows are limited by the amount of offgas available.
- The sizes and parameterization of the units are independent of the cell voltage. Identical system costs are assumed.

3.1. Feedstock

In addition to climate-neutral electricity, the primary feedstocks of the PtL-process are H_2O , CO_2 and air. All three mass flows depend only on the cell voltage and implemented with variables. Figure 3 shows the piecewise linear models of the feedstock flows.

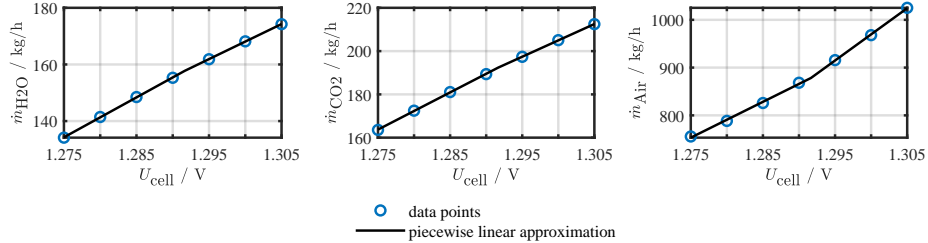


Figure 3: Piecewise-linear approximations for feedstocks as a function of the cell voltage U_{cell} . Left: 2 lines, $RMSE = 0.25 \%$. Center: 2 lines, $RMSE = 0.25 \%$. Right: 2 lines, $RMSE = 0.75 \%$.

3.2. System Power & FT-products

The parameters which significantly influence the overall process's performance are the system power P_{sys} and the massflow of FT-products $\sum_v \dot{m}_{\text{prod},v}$. Figure 4 shows the simulated data points and the model with piecewise linear approximated lines as a function of cell voltage U_{cell} . Both P_{sys} and product output increase with higher cell voltage. The model on the left side in Figure 4 describes the system's power consumption. P_{sys} represents the required power to run the co-SOEC, circulation pumps, valves, and control equipment, and to cover losses. The power consumption of utilities is considered in the modeling of the objectives in Section 3.5. Figure 4 on the right shows the product flow

downstream of the FT-reactor as the sum of the fractions FT-wax, diesel and naphtha.

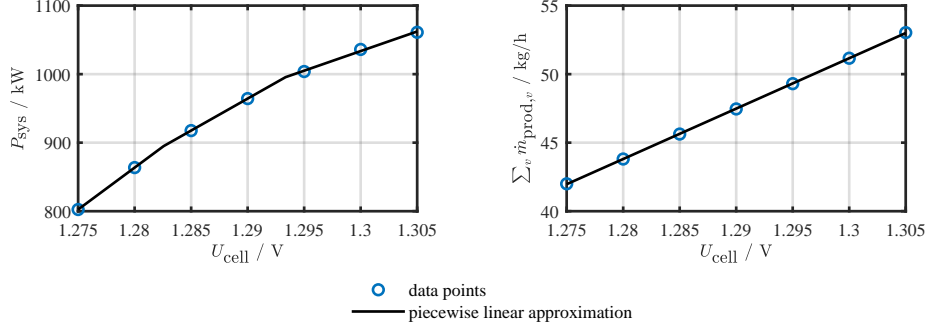


Figure 4: Piecewise-linear approximations of P_{sys} (left) and massflow of all FT-products (right) as a function of the cell voltage U_{cell} . Left: 3 lines, $RMSE = 0.43\%$. Right: 1 line, $RMSE = 0.19\%$

The composition of the fractions changes depending on the cell voltage. Figure 5 shows the absolute and relative share of the product flows. The percentage of FT-wax increases with increasing cell voltage. With an almost unchanged share of diesel, the share of naphtha is reduced simultaneously. Since we subsequently relate the production costs to all FT-products, the relative share of the fractions is not considered further.

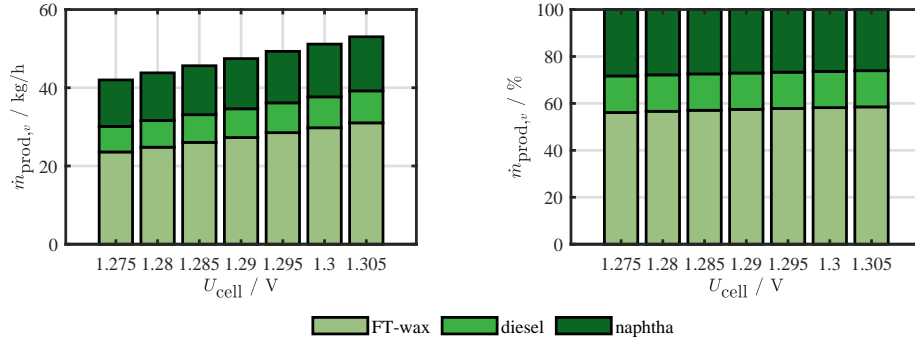


Figure 5: Absolute and relative product composition as a function of cell voltage U_{cell} .

3.3. Streams

The stream parameters T^{in} , T^{out} and F are dependent on the cell voltage. For each parameter, a piecewise linear approximation is generated. Figure 6 shows the results from process simulation and the piecewise linear approximation for stream H9. In this case, all parameters increase with increasing cell voltage. All other stream models can be found in the supplementary material.

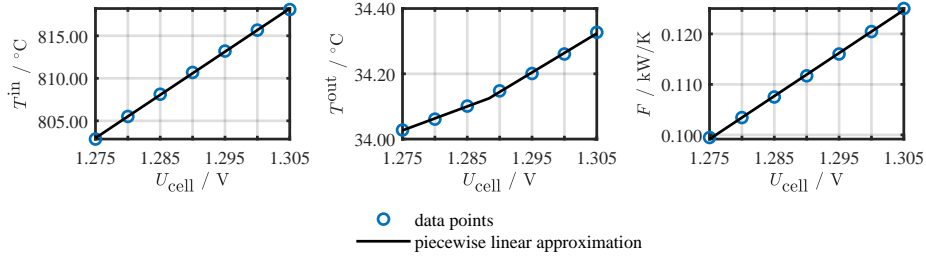


Figure 6: Piecewise-linear approximation of Stream H9. Left: 1 segment, $RMSE = 0.55\%$. Center: 2 segments, $RMSE = 0.90\%$. Right: 1 segment, $RMSE = 0.83\%$.

Table 2 summarizes the stream parameters' bounds for all streams. The stream parameters with brackets are variable and implemented depending on the cell voltage. Values without brackets are independent of cell voltage and constant. Especially for processes that require defined inlet and outlet conditions, the temperatures remain constant and only the flow capacity changes. This can be seen in the stream data of streams H12 and H4-H6 of the FT-reactor and upgrading. Stream parameters in square brackets are variable and depend on the cell voltage. The minimum and maximum values from the process simulation are given. The overall heat transfer coefficients were assumed to be $U = 0.5 \text{ kW}/(\text{m}^2 \text{ K})$ for all streams.

Table 2: Stream data: inlet, outlet temperature and flow capacity. The bounds for variable defined stream parameters are shown in square brackets.

Stream	$T^{\text{in}} / ^\circ\text{C}$	$T^{\text{out}} / ^\circ\text{C}$	$F / \text{kW/K}$
H1	40.0	35.0	[1.71, 2.16]
H2	[127.9, 131.1]	[34.0, 35.0]	[0.09, 0.12]
H3	[169.8, 174.1]	[34.0, 35.0]	[0.09, 0.12]
H4	210.0	190.0	[0.27, 0.28]
H5	190.0	120.0	[0.56, 0.58]
H6	120.0	30.0	[0.48, 0.50]
H7	[45.4, 57.0]	31.0	[2.35, 2.95]
H8	138.9	137.9	[59.60, 94.40]
H9	[805.2, 825.5]	[34.0, 35.0]	[0.10, 0.13]
H10	[49.5, 50.7]	[34.0, 35.0]	[0.65, 0.88]
H11	101.8	30.0	[0.51, 0.64]
H12	190.0	188.0	[76.88, 80.45]
C1	[318.0, 319.2]	[825.0, 870.5]	[0.14, 0.18]
C2	116.9	124.2	[20.02, 25.12]
C3	[57.3, 58.8]	825.0	[0.25, 0.33]
C4	137.9	139.9	[105.77, 142.64]
C5	138.9	[426.6, 449.4]	[0.10, 0.11]
C6	35.0	[115.9, 145.4]	[0.05, 0.06]
C7	20.3	[189.5, 199.6]	[0.15, 0.21]

3.4. Combustion System

The stream parameters of the CS are independent of the cell voltage; thus, no piecewise linear approximation is needed. Table 3 summarizes all stream parameters and heat transfer coefficients. The exhaust stream’s inlet temperature corresponds to the combustion chamber’s outlet temperature. An upper technical limit of 900 °C was chosen for all three streams. The outlet temperature can vary between 100 °C and 890 °C. The boundaries of the heat capacity flows were selected to guarantee that a sufficient amount of offgas is available for combustion. All overall heat transfer coefficients were assumed to be $U = 0.5 \text{ kW}/(\text{m}^2 \text{ K})$.

Table 3: Stream data with limits for inlet, outlet temperature and flow capacity.

Stream	$T^{\text{in}} / ^\circ\text{C}$	$T^{\text{out}} / ^\circ\text{C}$	$F / \text{kW/K}$
CS1	900.0	[100, 890]	[59.60, 94.40]
CS2	900.0	[100, 890]	[0.10, 0.13]
CS3	900.0	[100, 890]	[0.65, 0.88]

3.5. Objectives

Considering objective functions describing efficiency and costs simultaneously makes sense when optimizing energy conversion systems [16]. These objective functions are commonly antagonistic, allowing multiple optimal solutions to be represented as a Pareto front. The fuel production costs are minimized and the PtL-efficiency is maximized. The two objective functions reflect the trade-off between efficiency and productivity.

In Bezug auf Gleichung 1

3.5.1. PtL-Efficiency

The objective to maximize the PtL-efficiency η_{PtL} is defined by Equation (2) as the ratio of chemically bounded energy to electrical energy input.

$$\max \eta_{\text{PtL}} = \frac{\dot{H}_{\text{prod}}}{P_{\text{el}}} = \frac{\sum_v \dot{m}_{\text{prod},v} h_{\text{prod},v}}{P_{\text{sys}} + \sum_j \varepsilon_{\text{hu}} q_{\text{hu},j} + \sum_i \varepsilon_{\text{cu}} q_{\text{cu},i}} \quad (2)$$

The numerator describes the chemically bounded energy of the FT-products downstream of the separation. The denominator represents the total electrical energy input P_{el} . Both the hot and cold utilities are electrified. The coefficient of performance ε describes the electrical-to-thermal energy input ratio.

The PtL-efficiency from Equation (2) forms a non-linear correlation of the optimization variables for the chemically bounded energy in the product \dot{H}_{prod} and the electrical energy required P_{el} . The points in Figure 7 on the right show the non-linear function of the PtL-efficiency. Using MILP requires a piecewise-linear approximation. In this case, we used simplices on a regular grid with 4 x 4 points, see Figure 7 on the left. With 18 simplices, the objective can be approximated with sufficient accuracy at an RMSE of 0.61 %.

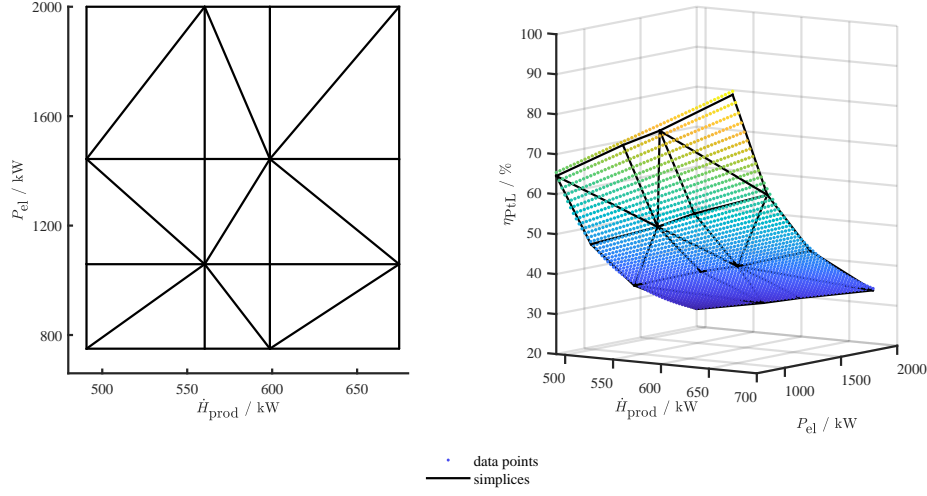


Figure 7: Piecewise-linear approximation with 18 simplices of the PtL-efficiency η_{PtL} as a function of chemically bounded energy in the produced fuels \dot{H}_{fuel} and electricity demand P_{el} . $RMSE = 0.61\%$.

3.5.2. Production Costs

The objective to minimize the specific production costs c_{prod} is defined according to Equation (3) and describes the ratio of total annual costs to product output.

$$\min c_{\text{prod}} = \frac{TAC}{\sum_v t \dot{m}_{\text{prod},v}} = \frac{CAPEX + OPEX}{\sum_v t \dot{m}_{\text{prod},v}} \quad (3)$$

The TAC are composed of annual capital expenses $CAPEX$ and operational expenditures $OPEX$. According to Equation (4), the $CAPEX$ comprises the investment costs for the system $CAPEX_{\text{sys}}$ and the heat exchanger network $CAPEX_{\text{HEN}}$. The investment costs for the system are calculated according to Equation (5) and include all relevant investments related to the PtL-plant, excluding the costs for the heat exchanger network. The annualized investment costs for the heat exchanger network are calculated according to Yee & Grossman [21] with Equation (6). Fixed costs for all heat exchangers and variable costs proportional to the heat exchanger area are considered. The investment annualization factor can be expressed as $AF_{\text{inv}} = 1/a$. Where a is the depreciation period in years. In contrast to linear depreciation, other options are also possible [26].

$$CAPEX = CAPEX_{\text{sys}} + CAPEX_{\text{HEN}} \quad (4)$$

$$CAPEX_{\text{sys}} = AF_{\text{inv}} C_{\text{sys}} \quad (5)$$

$$\begin{aligned}
CAPEX_{\text{HEN}} = AF_{\text{inv}} & \left[\underbrace{\sum_i \sum_j \sum_k c_{\text{v,hex}} \left(\frac{q_{ijk}}{U_{ij} LMTD_{ijk}} \right)^\beta}_{\text{variable HEX stream costs}} \right. \\
& + \underbrace{\sum_i c_{\text{v,hex}} \left(\frac{q_{\text{cu},i}}{U_{\text{cu},i} LMTD_{\text{cu},i}} \right)^\beta}_{\text{variable HEX cold utility costs}} + \underbrace{\sum_j c_{\text{v,hex}} \left(\frac{q_{\text{hu},j}}{U_{\text{hu},j} LMTD_{\text{hu},j}} \right)^\beta}_{\text{variable HEX hot utility costs}} \\
& \left. + \underbrace{\sum_i \sum_j \sum_k c_{\text{f,hex}} z_{ijk} + \sum_i c_{\text{f,hex}} z_{\text{cu},i} + \sum_j c_{\text{f,hex}} z_{\text{hu},j}}_{\text{fixed investment costs hex}} \right] \quad (6)
\end{aligned}$$

According to Equation (7), the operational expenses are composed of feedstock and electricity costs. The OPEX depend on the annual full load hours t and are usually depreciated within one year, which results in an operational annualization factor of $AF_{\text{op}} = 1$.

$$\begin{aligned}
OPEX = AF_{\text{op}} t & \left\{ \underbrace{\sum_w c_{\text{f}} \dot{V}_{\text{f}}}_{\text{feedstock costs}} \right. \\
& \left. + c_{\text{el}} \left[\underbrace{P_{\text{sys}} + \left(\sum_j \varepsilon_{\text{uh}} q_{\text{uh},j} + \sum_i \varepsilon_{\text{uc}} q_{\text{uc},i} \right)}_{\text{electricity costs}} \right] \right\} \quad (7)
\end{aligned}$$

The nonlinear objective of the minimum fuel production costs is piecewise-linear approximated and transferred to MILP. Figure 8 shows the approximation in its valid domain on a 3 x 3 grid. With only eight simplices, an *RMSE* of 0.37 % can be achieved.

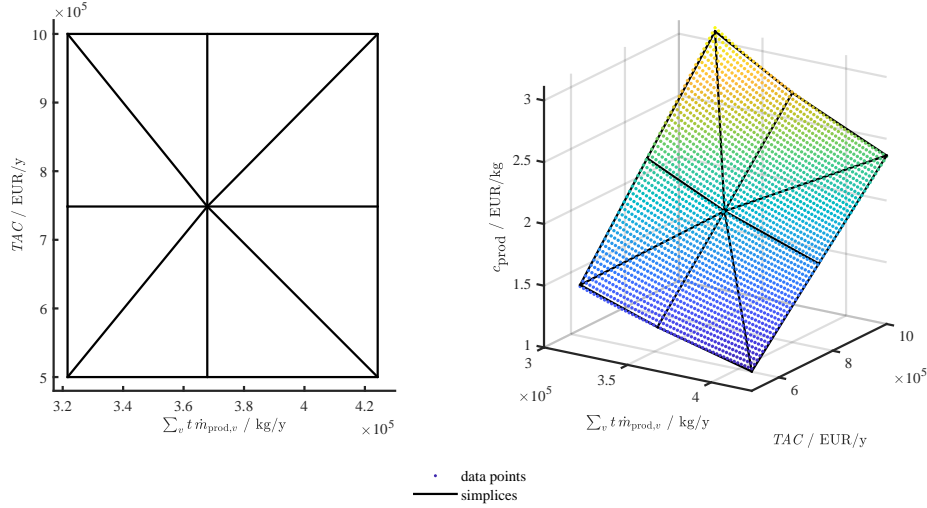


Figure 8: Piecewise-linear approximation with eight simplices of production costs c_{prod} as a function of the total annual costs TAC and that total product flow $\sum_v \dot{m}_{\text{prod},v}$. $RMSE = 0.37\%$.

The three nonlinear terms of the variable heat exchanger costs in Equation (7) are piecewise-linear approximated analogously to the procedure of Huber et al. [24]. Accordingly, the stream and utility heat exchanger area correlations are approximated by superpositioned planes and transferred to MILP without additional binary variables.

3.6. Simulation Parameters

3.6.1. Costs

As the number of full load hours of the plant increases, the net production costs decrease [27]. Like the authors in [27, 28, 29], we also assume $t = 8000$ h/y full load hours per year. All components are depreciated linearly within 20 years resulting in an annualization factor of $AF_{\text{inv}} = 1/20$.

The fixed investment costs have been estimated by the project partners responsible for the economic viability to be $C_{\text{sys}} = 10\,000\,000$ €. This estimate assumes that the cost of the central components will decrease significantly due to technological advances [12]. In the papers of G. Herz et al. [28] and D.H. König et al. [30], costs in the range of 9 600 000 € and 22 000 000 € have been predicted, which legitimizes the intra-project estimation.

The feedstock for the production of synthetic fuels can be reduced to H_2O , CO_2 rich exhaust gas and air in a simplified form. Table 4 lists the corresponding cost factors c_f .

Table 4: Feedstock cost factors.

f	feedstock	$c_f/\text{€}/\text{t}$	reference
1	H ₂ O	3.54	mean for Europe in [31]
2	CO ₂	50 ¹	EU ETS 2026-30 [32]
3	Air	0 ²	

¹ CO₂ treatment is considered in C_{sys} and P_{sys} .

² Air is available free of charge. The process was designed to use air with ambient conditions.

The goal of producing CO₂-neutral fuels can only be achieved by using electricity produced in a CO₂-neutral way. The electricity required for this will be generated from a mix of wind and solar PV. At a projected plant location in Europe, an average electricity price of $c_{\text{el}} = 20 \text{ €}/(\text{MW h})$ is assumed, according to J.L.L.C.C. Janssen et al. [33].

3.7. Heat Exchanger Network

The heat exchanger network was defined with $N_{\text{st}} = 3$ stages for heat exchange and a minimum temperature difference of $\Delta T_{\text{min}} = 1 \text{ K}$.

Air coolers are used as cold utilities. Since the environment is used as a heat sink, a coefficient of performance of $\varepsilon_{\text{uc}} = 0.05$ is assumed to cover evaporation losses and mechanical work. Electrical heating elements with a coefficient of performance of $\varepsilon_{\text{uh}} = 1.05$ are used as hot utilities.

The cost parameters for the heat exchangers in the heat exchanger network have been determined based on the DACE Price Booklet [34]. We have selected stainless plate heat exchangers made of AISI 316. The cost parameters are $c_{\text{f,hex}} = 1013.6 \text{ €/y}$ and $c_{\text{v,hex}} = 61.8 \text{ €}/(\text{m}^2 \beta \text{ y})$ with a degressive cost exponent of $\beta = 0.8$.

3.8. Piecewise-linear Approximation

Superpositioned lines, planes or simplices were added to all piecewise-linear models until an RMSE of less than 1 % was achieved. When approximating with simplices, care was taken to fully utilize the logarithmic encoding with respect to the selected grid points.

3.9. Implementation

The multiobjective optimization problem was solved using the adapted epsilon constraint method shown in Equation (1). For that, η_{PtL} was implemented as $-f_1(\mathbf{x})$ and c_{prod} as $f_2(\mathbf{x})$.

All optimization problems were coded in MATLAB 2020b [35]. YALMIP R20210331 has been used as an interface between MATLAB and the MILP solver [36]. Gurobi 10.0.0 is used as the MILP Solver [37]. A MIP of less than 1 % was defined as a termination criterion for the solver. The calculations were performed on a 64-core server (AMD EPYC 7702P) with 265 GB of RAM.

4. Results

The coupled optimization results are compared with two conventionally designed plants without optimization to quantify the presented method's potential. The following assumptions are made for the conventional plant design:

- The two operating points are set at the extreme cell voltage values.
- The HEN is designed empirically following the PINCH rules.
- The stream parameters of the CS are chosen empirically.

Figure 9 shows the two solutions of the conventional design without optimization and the Pareto front of the coupled optimization as a function of the cell voltage. The different cell voltages are color-coded. The Pareto front is constructed with 42 points. On average, a solver time of 465.7 s per point was achieved. All 42 points were calculated within 23.8 hours. More details can be found in Appendix A. The gaps in areas of high production costs result from the solver timeout. Within 12 hours, no solutions with a MIP gap of less than 1 % could be found. A high cell voltage generally leads to low efficiency and production costs. A low cell voltage, on the other hand, leads to increased efficiency and, at the same time, high production costs. The two objective functions are intensely antagonistic, at least near the optimum.

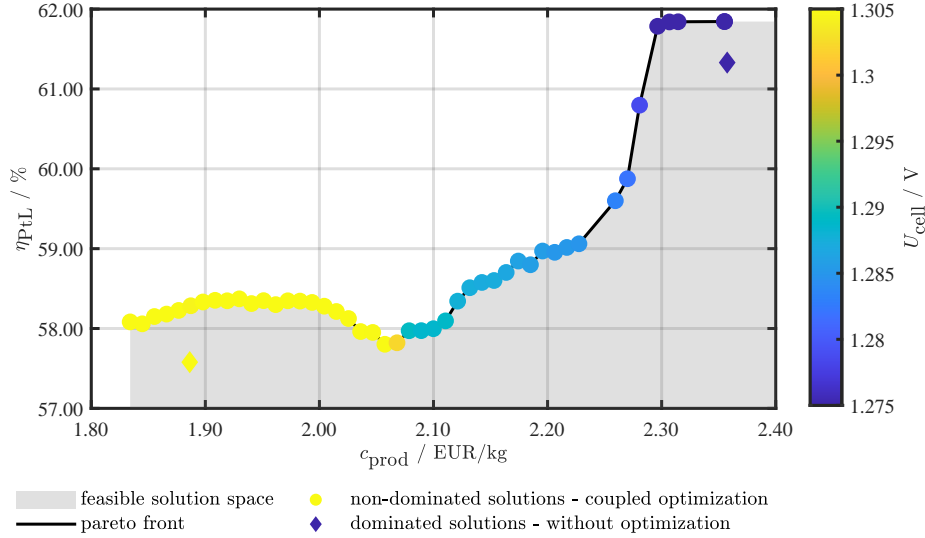


Figure 9: Non-dominated solutions and Pareto front of coupled optimization (circles). Dominated solutions of the conventional approach (diamonds).

Table 5 shows the characteristic values for the empirical design approach without optimization. Further, the characteristic values at the corners of the Pareto front from the coupled optimization are shown. The associated stream plots can be found in Appendix B.

Production costs at a cell voltage of 1.275 V are almost identical at 2.355 €/kg compared to 2.358 €/kg. The efficiency can be increased by 0.514 percentage points (0.84 %). Both HENs use 27 heat exchangers. Whereas in the empirical design, one is used as hot utility HEX. Further, it is noticeable that the major improvement results from the lower power of the cold utilities. The power can be reduced from 222.25 kW to 155.62 kW.

At a cell voltage of 1.305 V, the production cost can be reduced by 5.22 ct (2.77 %) while increasing the efficiency by 0.504 percentage points (0.88 %). Compared to the HEN of the coupled optimization with 20 HEX, the empirical design requires 34 HEX. The lower cost of HEN is a crucial driver for the cost savings. It should also be pointed out that only one of the three CS is required for the optimized HEN; see Figure B.14 in Appendix B. This may result in cost reductions in system costs. However, these will not be discussed further in this paper.

Table 5: Comparison of extreme values from coupled optimization and empirical design without optimization.

variable	unit	empirical	optimization	empirical	optimization
U_{cell}	V	1.275	1.275	1.305	1.305
c_{prod}	€/kg	2.358	2.355	1.886	1.834
η_{PtL}	%	61.330	61.844	57.579	58.083
$CAPEX_{\text{sys}}$	€/y	500 000	500 000	500 000	500 000
$CAPEX_{\text{HEN}}$	€/y	39 680	40 540	45 980	25 990
$OPEX$	€/y	200 660	199 140	260 860	259 880
TAC	€/y	740 340	739 680	806 640	785 870
n_{HEX}		27	27	34	20
$\sum_i q_{\text{cu},i}$	kW	222.25	155.62	378.63	255.76
$\sum_j q_{\text{hu},j}$	kW	5.90	0	0	0
$\sum_i \sum_j \sum_k q_{i,j,k}$	kW	717.34	723.19	890.26	890.24

The shape of the Pareto front, whether convex or non-convex, provides information about the nature of the underlying problem and the trade-offs between the different objectives. A convex Pareto front indicates clear dominant solutions where an improvement in one objective necessarily leads to a degradation of the other. A distinct optimal solution usually combines the best values for all objectives in such cases. In contrast, in this case, a non-convex Pareto front indicates no unambiguously dominant solution and different combinations of objective functions represent equivalent alternatives. Looking at the Pareto front from Figure 9, we find that the efficiency remains nearly constant in the low-production cost region at about 58 %. For a cell voltage of $U_{\text{cell}}^{\text{min}} = 1.305$ V, the production costs vary between 1.834 €/kg and 2.057 €/kg, while the efficiency varies between 57.803 % and 58.371 %. In our case, an identical cell

voltage means that the solutions differ only in the HEN design and the parameterization of the CS. It can be concluded that, especially in this range, the influence of the design variables has significant effects on the production costs with negligible effects on efficiency. Similarly, in the high production cost range, a significant increase in efficiency can be seen with a minor increase in production cost. From 2.068 €/kg to 2.297 €/kg, the PtL efficiency increases by 3.963 percentage points to 61.785 %. However, all solutions show different cell voltages in this interval. It can be concluded that the choice of cell voltage has a more significant impact on the objective functions than the choice of HEN and the parameterization of the CS. In the range of highest production costs between 2.297 €/kg and 2.355 €/kg, four solutions with a cell voltage of $U_{\text{cell}}^{\text{min}} = 1.275 \text{ V}$ are found. The efficiency varies only by about 0.096 % in the nearly horizontal zone increasing from 61.785 % . The production costs, on the other hand, differ by up to 5.863 ct/kg.

The results show that in our use case, the cell voltages of the Pareto optimal solutions do not change in the horizontal section at the beginning and end of the Pareto front. In this region, the HEN design and the parameterization of the CS are of crucial importance. However, in the near-vertical part of the Pareto front, the choice of cell voltage significantly affects the objective functions. The HEN design and the parameterization of the CS have only a minor influence. Therefore, the coupled optimization of the operating parameters and the HEN is essential if the impact of different design parameters cannot be estimated a priori.

5. Conclusion

In this paper, we present a method that enables coupled optimization of design and operating parameters in the heat exchanger network (HEN) problem. The coupling is realized by modeling an operating point dependent behavior of stream parameters inlet, outlet temperature and flow capacity. All nonlinearities are approximated with piecewise linear approximations to keep the problem tractable and to leverage the potential of fast MILP solvers. The transfer to MILP is done highly efficiently using logarithmic coding. The method is applied to a novel 1 MW PtL-process. Selecting the cell voltage of the co-SOEC and the combustion system’s (CS) parameterization is crucial for the process design. These complex processes cannot be evaluated purposefully based on only one objective. Therefore, multi-criteria optimization of PtL-efficiency and production costs provides a robust decision basis for comprehensive process assessment.

Our results show that coupled optimization leads to better results than the conventional design approach. Higher efficiencies can be achieved with lower production costs at the same time. By modeling the systems’ operational and design parameters, it is possible to optimize the overall process comprehensively and to calculate a Pareto front that reflects the trade-off of the objective functions. The shape of the Pareto front provides valuable insight into the nature

of the problem. In this paper, a non-convex Pareto front was observed, suggesting that no uniquely dominant solution and different combinations of objectives represent equivalent alternatives. Efficiency remained approximately constant in the low-production cost region. This indicates that the influence of HEN and CS parameters significantly affects production costs, while the effects on efficiency are negligible. On the other hand, in the high production cost area, a slight increase in production cost resulted in a significant improvement in efficiency. The choice of cell voltage was found to have a more substantial impact on the objective functions than the choice of HEN and the parameterization of the CS. The results underline the relevance of coupled optimization, especially when the effects of the different operational and design parameters cannot be estimated a priori.

With our method, we close a research gap by coupled optimization of operating and design parameters. Simultaneously considering several objective functions enables a comprehensive analysis of the solution space based on Pareto fronts. This allows synergy effects to be exploited and optimal solutions to be identified highly efficiently. Further research and analysis could focus on implementing additional operational or design variables to improve the overall performance and sustainability of the PtL-plant. With this work, we can contribute to the highly efficient and cost-effective production of synthetic fuels, which will promote timely large-scale industrial production and reduce emissions in the long run.

References

- [1] International Energy Agency, CO2 Emissions in 2022: Global Energy Review, Technical Report, 2022. URL: <https://www.iea.org/reports/co2-emissions-in-2022>.
- [2] International Energy Agency, Global EV Outlook 2022, Technical Report, 2022. URL: <https://www.iea.org/reports/global-ev-outlook-2022>.
- [3] S. Hänggi, P. Elbert, T. Bütler, U. Cabalzar, S. Teske, C. Bach, C. Onder, A review of synthetic fuels for passenger vehicles, *Energy Reports* 5 (2019) 555–569. doi:10.1016/j.egy.2019.04.007.
- [4] R. Pinsky, P. Sabharwall, J. Hartvigsen, J. O’Brien, Comparative review of hydrogen production technologies for nuclear hybrid energy systems, *Progress in Nuclear Energy* 123 (2020) 103317. doi:10.1016/j.pnucene.2020.103317.
- [5] M. Marchese, E. Giglio, M. Santarelli, A. Lanzini, Energy performance of Power-to-Liquid applications integrating biogas upgrading, reverse water gas shift, solid oxide electrolysis and Fischer-Tropsch technologies, *Energy Conversion and Management: X* 6 (2020) 100041. doi:10.1016/j.ecmx.2020.100041.

- [6] Siemens energy, Haru Oni: Base camp of the future, 2023. URL: <https://www.siemens-energy.com/global/en/news/magazine/2022/haru-oni.html>.
- [7] Norsk e-fuel, Driving the transition to renewable aviation today, 2023. URL: <https://www.norsk-e-fuel.com/>.
- [8] D. S. Marlin, E. Sarron, O. Sigurbjörnsson, Process Advantages of Direct CO₂ to Methanol Synthesis, *Frontiers in Chemistry* 6 (2018) 446. doi:10.3389/fchem.2018.00446.
- [9] INERATEC, Industrial Power-to-Liquid Pioneer Plant in Germany, 2022. URL: <https://planet-a.com/startups/ineratec/>.
- [10] J. Zhao, Y. Yu, H. Ren, M. Makowski, J. Granat, Z. Nahorski, T. Ma, How the power-to-liquid technology can contribute to reaching carbon neutrality of the China's transportation sector?, *Energy* 261 (2022) 125058. doi:10.1016/j.energy.2022.125058.
- [11] T. Ngan Do, C. You, J. Kim, A CO₂ utilization framework for liquid fuels and chemical production: techno-economic and environmental analysis, *Energy & Environmental Science* 15 (2022) 169–184. doi:10.1039/D1EE01444G, publisher: Royal Society of Chemistry.
- [12] F. Ueckerdt, C. Bauer, A. Dirnaichner, J. Everall, R. Sacchi, G. Luderer, Potential and risks of hydrogen-based e-fuels in climate change mitigation, *Nature Climate Change* 11 (2021) 384–393. doi:10.1038/s41558-021-01032-7, number: 5 Publisher: Nature Publishing Group.
- [13] M. Ram, T. Galimova, D. Bogdanov, M. Fasihi, A. Gulagi, M. Micheli, K. Crone, C. Breyer, Powerfuels in a Renewable Energy World: Global Volumes, Costs, and Trading 2030 to 2050 (2020). doi:10.13140/RG.2.2.32687.56487, publisher: Lappeenranta – Lahti University of Technology LUT.
- [14] U.S. Energy Information Administration, U.S. Total Gasoline Wholesale/Resale Price by Refiners (Dollars per Gallon), 2023. URL: <https://www.eia.gov/petroleum/data.php>.
- [15] F. Ueckerdt, A. Odenweller, E-Fuels - Aktueller Stand und Projektionen, Technical Report, Potsdam-Institut für Klimafolgenforschung, 2023.
- [16] A. A. Al-Rashed, M. Afrand, Multi-criteria exergoeconomic optimization for a combined gas turbine-supercritical CO₂ plant with compressor intake cooling fueled by biogas from anaerobic digestion, *Energy* 223 (2021) 119997. doi:10.1016/j.energy.2021.119997.
- [17] Y. Cao, H. A. Dhahad, H. M. Hussen, A. E. Anqi, N. Farouk, A. Issakhov, Development and tri-objective optimization of a novel biomass to power and hydrogen plant: A comparison of fueling with biomass gasification

- or biomass digestion, *Energy* 238 (2022) 122010. doi:10.1016/j.energy.2021.122010.
- [18] T. Hai, K. Hikmat Hama Aziz, J. Zhou, H. A. Dhahad, K. Sharma, S. Fahad Almojil, A. Ibrahim Almohana, A. Fahmi Alali, T. Ismail Kh, S. Mehrez, A. Abdelrahman, -Neural network-based optimization of hydrogen fuel production energy system with proton exchange electrolyzer supported nanomaterial, *Fuel* 332 (2023) 125827. doi:10.1016/j.fuel.2022.125827.
 - [19] C. Wang, S. Guo, H. Pei, Y. He, D. Liu, M. Li, Rolling optimization based on holism for the operation strategy of solar tower power plant, *Applied Energy* 331 (2023) 120473. doi:10.1016/j.apenergy.2022.120473.
 - [20] M. Linnhoff, Introduction to pinch technology, Targeting House, Gadbrook Park, Northwich, Cheshire, CW9 7UZ, England (1998).
 - [21] T. F. Yee, I. E. Grossmann, Simultaneous optimization models for heat integration—II. Heat exchanger network synthesis, *Computers & Chemical Engineering* 14 (1990) 1165–1184. doi:10.1016/0098-1354(90)85010-8.
 - [22] M. Escobar, J. O. Trierweiler, Optimal heat exchanger network synthesis: A case study comparison, *Applied Thermal Engineering* 51 (2013) 801–826. doi:10.1016/j.applthermaleng.2012.10.022.
 - [23] Z. Liu, L. Yang, S. Yang, Y. Qian, An extended stage-wise superstructure for heat exchanger network synthesis with intermediate placement of multiple utilities, *Energy* 248 (2022) 123372. doi:10.1016/j.energy.2022.123372.
 - [24] D. Huber, F. Birkelbach, R. Hofmann, HENS Unchained: MILP Implementation of Multi-Stage Utilities with Stream Splits, Variable Temperatures and Flow Capacities, *Energies* 16 (2023) 4732. doi:10.3390/en16124732.
 - [25] J. P. Vielma, G. L. Nemhauser, Modeling disjunctive constraints with a logarithmic number of binary variables and constraints, *Mathematical Programming* 128 (2011) 49–72. doi:10.1007/s10107-009-0295-4.
 - [26] D. Halmschlager, A. Beck, S. Knöttner, M. Koller, R. Hofmann, Combined optimization for retrofitting of heat recovery and thermal energy supply in industrial systems, *Applied Energy* 305 (2022) 117820. doi:10.1016/j.apenergy.2021.117820.
 - [27] S. Adelung, Global sensitivity and uncertainty analysis of a Fischer-Tropsch based Power-to-Liquid process, *Journal of CO₂ Utilization* 65 (2022) 102171. doi:10.1016/j.jcou.2022.102171.
 - [28] G. Herz, C. Rix, E. Jacobasch, N. Müller, E. Reichelt, M. Jahn, A. Michaelis, Economic assessment of Power-to-Liquid processes – Influence of electrolysis technology and operating conditions, *Applied Energy* 292 (2021) 116655. doi:10.1016/j.apenergy.2021.116655.

- [29] V. Dieterich, A. Buttler, A. Hanel, H. Spliethoff, S. Fendt, Power-to-liquid *via* synthesis of methanol, DME or Fischer–Tropsch-fuels: a review, *Energy & Environmental Science* 13 (2020) 3207–3252. doi:10.1039/D0EE01187H.
- [30] D. H. König, M. Freiberg, R.-U. Dietrich, A. Wörner, Techno-economic study of the storage of fluctuating renewable energy in liquid hydrocarbons, *Fuel* 159 (2015) 289–297. doi:10.1016/j.fuel.2015.06.085.
- [31] EurEau, Europe’s Water in Figures: An overview of the European drinking water and waste water sectors, 2021. URL: <https://www.eureau.org/resources/publications/eureau-publications/5824-europe-s-water-in-figures-2021/file>.
- [32] IETA, GHG Market Sentiment Survey 2022, Technical Report, 2022. URL: <https://www.ieta.org/resources/Documents/IETA%20GHG%20Market%20Sentiment%20Survey%20Report%202022.pdf>.
- [33] J. Janssen, M. Weeda, R. J. Detz, B. van der Zwaan, Country-specific cost projections for renewable hydrogen production through off-grid electricity systems, *Applied Energy* 309 (2022) 118398. doi:10.1016/j.apenergy.2021.118398.
- [34] DACE price booklet: cost information for estimation and comparison, edition 35 ed., DACE Cost and Value, Nijkerk, 2021. OCLC: 1303572720.
- [35] The MathWorks Inc., MATLAB version: 9.13.0 (R2022b), 2022. URL: <https://www.mathworks.com>.
- [36] J. Löfberg, A toolbox for modeling and optimization in MATLAB, *Proceedings of the CACSD Conference* (2004) 289. doi:10.1109/CACSD.2004.1393890.
- [37] Gurobi Optimization, LLC, Gurobi Optimizer Reference Manual, 2023. URL: <https://www.gurobi.com>.

Statements and Declarations

Funding

This research was funded by the Austrian Research Promotion Agency (FFG) under grant number 884340 and TU Wien Bibliothek through its Open Access Funding Programme.

Competing Interests

The authors have no relevant financial or non-financial interests to disclose.

Authors Contributions

The method presented in this paper was developed by David Huber. Testing and evaluation was done by David Huber. The conceptualization of the paper was done by all authors. The first draft was written by David Huber. All authors contributed to the revision of the initial draft. Funding and supervision was done by René Hofmann. All authors read and approved the final manuscript.

Appendix A. Solver Time

Figure A.10 shows the solver time for the 42 points of the Pareto front as bar plot. The solver time refers to the time it takes the solver to find a solution within the defined MIP gap of 1 %. The mean solver time was 465.7 s. The total solver time was $8.5809 \cdot 10^4$ s or 23.8 h.

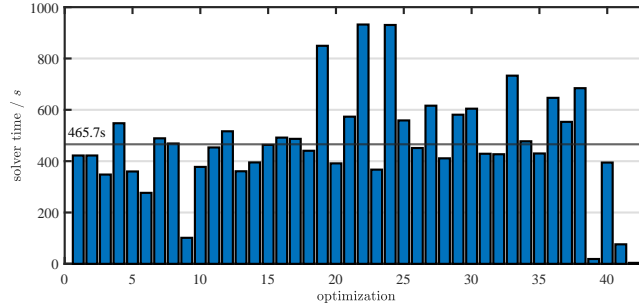


Figure A.10: Solver time for each optimization (blue bars) and mean solver time (black line).

Appendix B. Stream Plots

Figures B.11 and B.13 show the empirically constructed HENs for a cell voltage of $U_{\text{cell}} = 1.275$ V and $U_{\text{cell}} = 1.305$ V, respectively. In addition, Figures B.12 and B.14 show the HENs with the same cell voltage resulting from the coupled optimization. Based on the detailed results from Table 5, the corner points of the Pareto front have been used.

With the coupled optimization, the design of the combustion system (CS) is coupled with the optimization of the HEN, among other things. Accordingly, the outlet temperatures and flow capacities of the corresponding streams CS1-3 are implemented as variables. It can be seen that compared to the empirically defined designs, the outlet temperatures of stream CS1-3 are significantly higher. Du to the higher temperature differences, the heat exchanger surfaces can be reduced at the same performance, lowering costs.

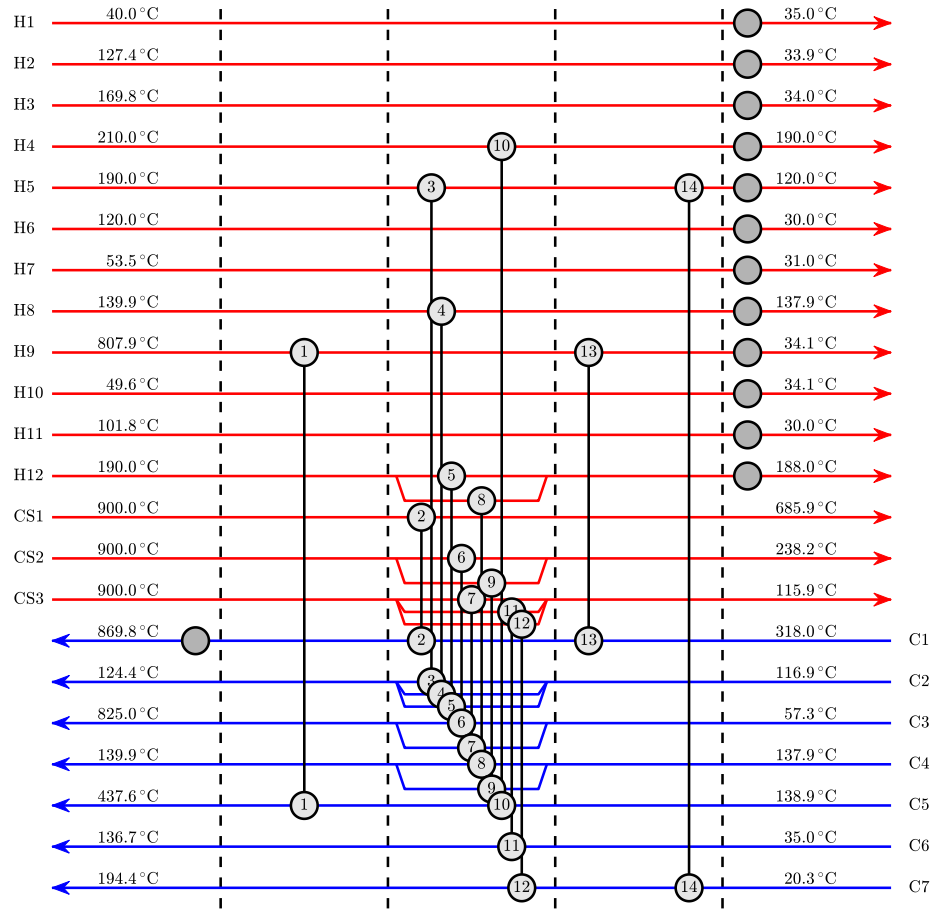


Figure B.11: Stream plot with 27 heat exchangers resulting from the empirical design without optimization. Characteristic figures: $\eta_{\text{PtL}} = 61.330\%$, $c_{\text{prod}} = 2.358 \text{ €/kg}$, $U_{\text{cell}} = 1.275 \text{ V}$.

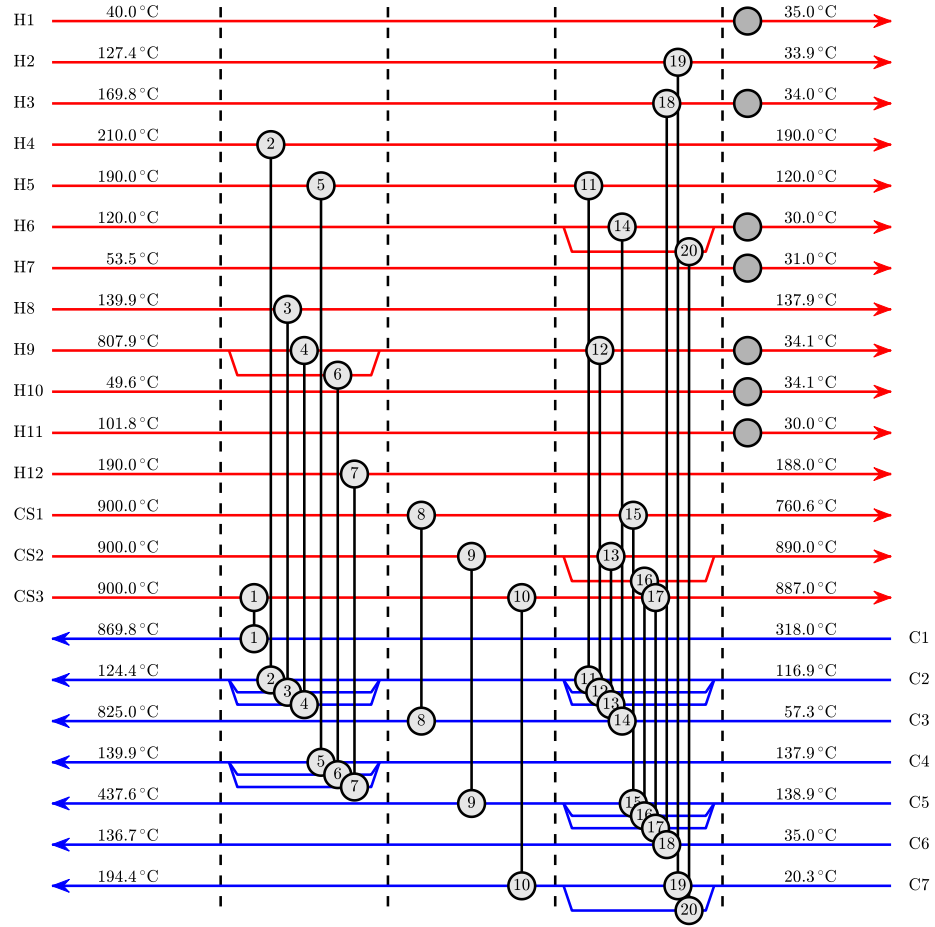


Figure B.12: Stream plot with 27 heat exchangers resulting from the coupled optimization.
Characteristic figures: $\eta_{\text{PtL}} = 61.844\%$, $c_{\text{prod}} = 2.355 \text{ €/kg}$, $U_{\text{cell}} = 1.275 \text{ V}$.

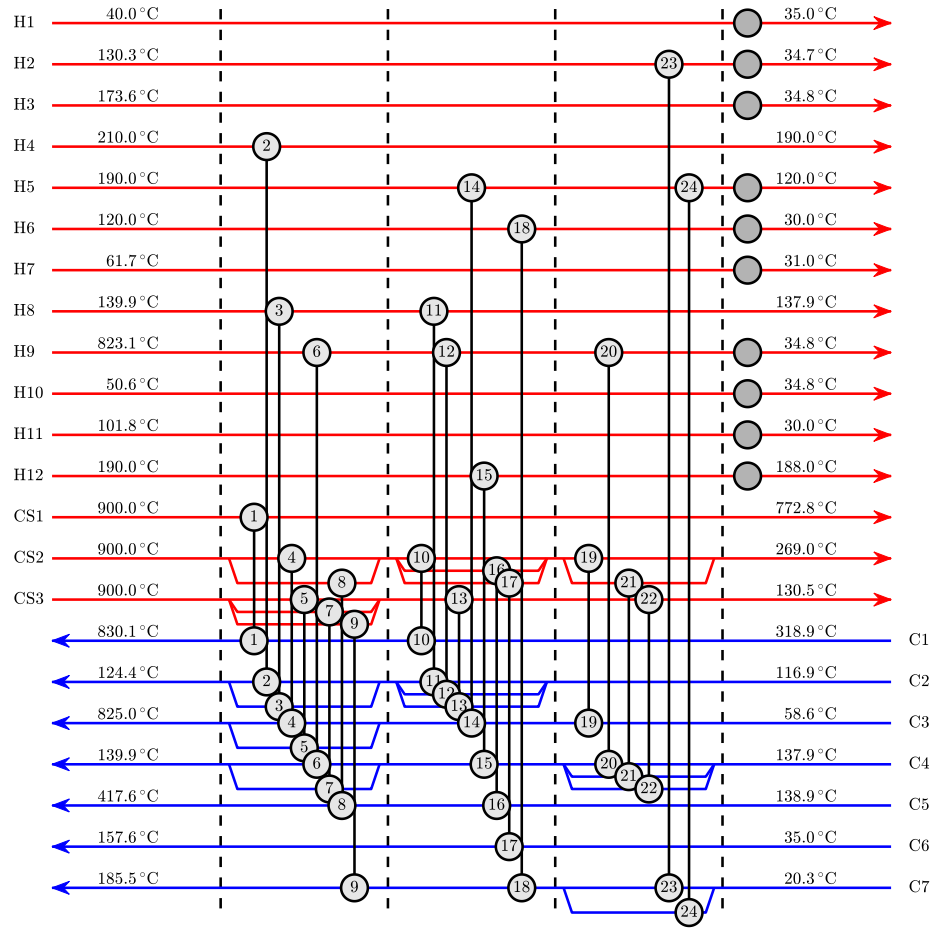


Figure B.13: Stream plot with 34 heat exchangers resulting from the empirical design without optimization. Characteristic figures: $\eta_{\text{PtL}} = 57.579\%$, $c_{\text{prod}} = 1.886 \text{ €/kg}$, $U_{\text{cell}} = 1.305 \text{ V}$.

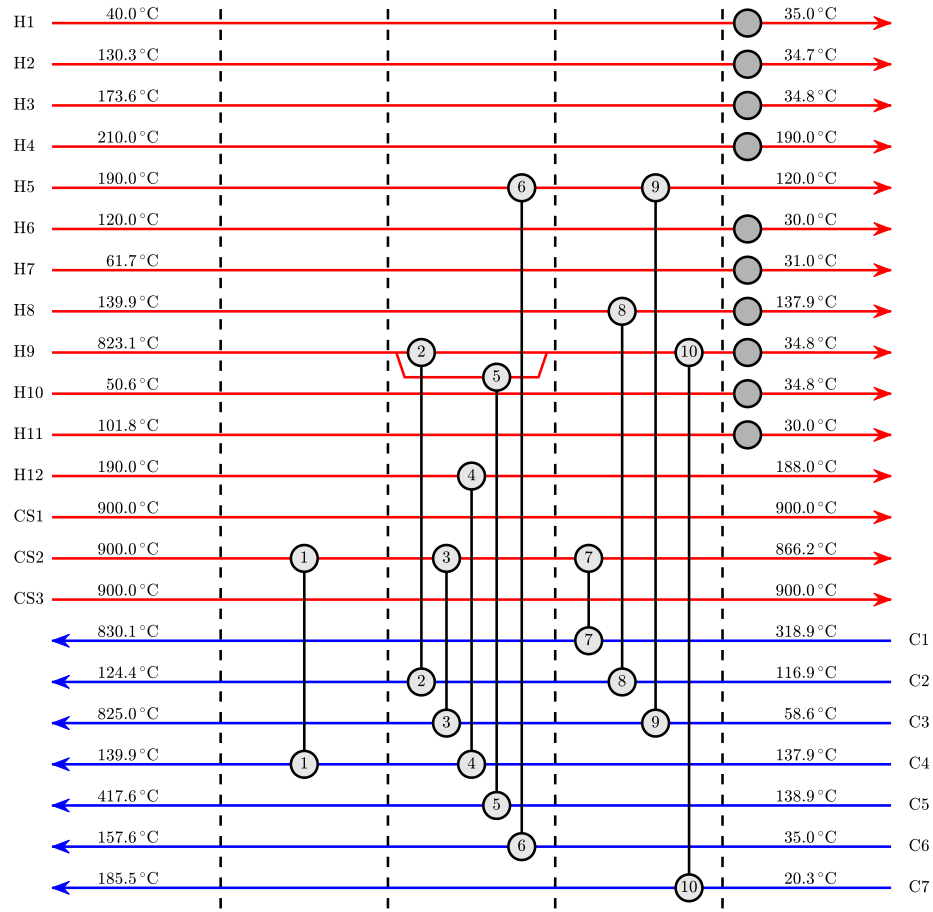


Figure B.14: Stream plot with 20 heat exchangers resulting from the empirical design without optimization. Characteristic figures: $\eta_{\text{PtL}} = 58.083\%$, $c_{\text{prod}} = 1.834 \text{ €/kg}$, $U_{\text{cell}} = 1.305 \text{ V}$.